Cosmic Masers: Proper Motion toward the Next-Generation Large Projects
Proceedings IAU Symposium No. 380, 2024
T. Hirota, H. Imai, K. Menten, & Y. Pihlström, eds.
doi:10.1017/S1743921323002636

Maser Activity of Large Molecules toward Sgr B2 North

Ci Xue[1], Anthony Remijan[2], Alexandre Faure[3] and Brett McGuire[1,2]

[1]Massachusetts Institute of Technology, Cambridge, MA 02139, USA. email: cixue@mit.edu

[2]National Radio Astronomy Observatory, Charlottesville, VA 22903, USA

[3]Université Grenoble Alpes, CNRS, IPAG, F-38000 Grenoble, France

Abstract. Single-dish observations at centimeter wavelengths have suggested that the Sgr B2 molecular cloud at the Galactic Center hosts weak maser emission from several large molecules. Here, we present the interferometric observations of the Class I methanol (CH_3OH) maser at 84 GHz, the methanimine (CH_2NH) maser at 5.29 GHz, and the methylamine (CH_2NH_2) maser at 4.36 GHz toward Sgr B2 North (N). We use a Bayesian approach to quantitatively assess the observed masing spectral profiles and the excitation conditions. By comparing the spatial origin and extent of maser emission from several molecular species, we find that the new maser transitions have a close spatial relationship with the Class I masers, which suggests a similar collisional pumping mechanism.

Keywords. ISM: molecules, Interstellar masers, Spectral line identification

1. Introduction

Common species exhibiting maser emission include, but are not limited to, OH, SiO, H_2O, H_2CO, NH_3, and CH_3OH. An empirical taxonomy based on pumping mechanisms classifies molecular masers into two categories (Cyganowski et al. 2009); Class I CH_3OH and H_2O masers are most often excited via collisions and tend to reside in shocked material associated with outflows and expanding HII regions, while Class II CH_3OH and OH masers are excited via radiation and are generally close to young stellar objects and luminous infrared sources. Recently, new maser species, such as HNCO and CH_2NH, have been discovered to exhibit compelling roles in inferring fine-scale structures and gas dynamics in the maser region (Chen et al. 2020; Gorski et al. 2021). The pumping mechanism of these new maser species, however, is less constrained, as is their relation to other common maser species. Observations of these species in maser-active regions that contain both known Class I and Class II masers are therefore critical as a first step in understanding their pumping mechanisms.

The high-mass star-forming region Sgr B2 (N) is one of the richest known sources for not only molecular discoveries but also maser activity from a diverse set of molecules (e.g. Walsh et al. 2014). In addition to the common maser species, Sgr B2 displays rare maser activity from complex molecules. The single-dish PRIMOS line-survey project has identified numerous species exhibiting maser activity at centimeter wavelengths (e.g. HNCNH, McGuire et al. 2012). The radiative transfer calculations also revealed that most emission lines of both $HCOOCH_3$ and CH_2NH detected in PRIMOS are weak masers amplifying the background radiation of Sgr B2(N) at cm wavelengths (Faure et al. 2014, 2018). However, the large $\sim 2.5' \times 2.5'$ field of view of PRIMOS at 5 GHz includes both the

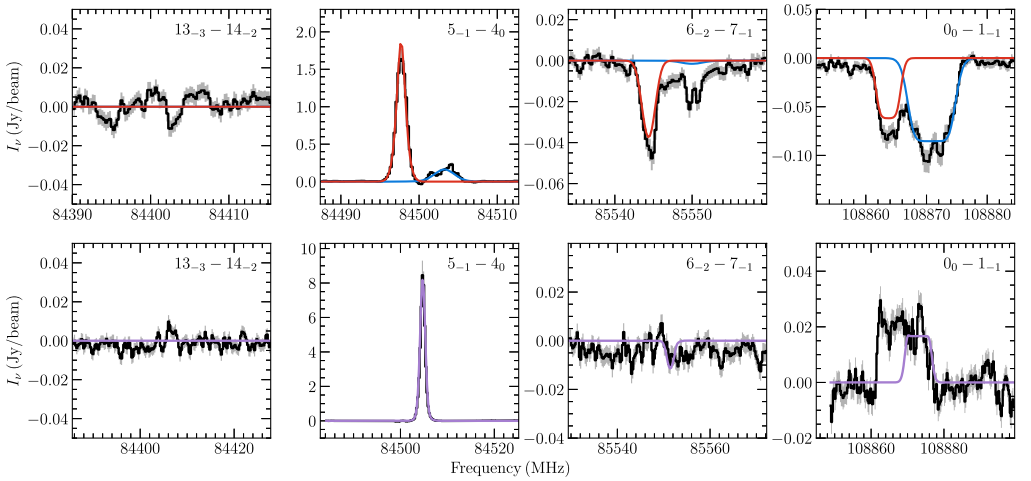

Figure 1. Observed and synthetic spectra of the E-type CH_3OH transitions. The observed spectra are shown in black with noise levels shaded in gray. The top panel shows the spectra extracted toward the CH_3OH-83 km s^{-1} spot, and the bottom panel shows the spectra extracted toward the brightest CH_3OH maser spot. The best-fit synthetic spectra are overlaid in colors, with the red trace representing the 83 km s^{-1} component, the blue trace representing the 64 km s^{-1} component, and the purple trace representing the 58 km s^{-1} components.

North and Main components of Sgr B2, complicating the interpretation of the spectral profiles. Therefore, it is crucial to have interferometric observations to disentangle in detail the various possible spatial components of maser emission.

We present a rigorous imaging study of maser emission from CH_3OH, CH_2NH, and CH_2NH_2 toward Sgr B2(N). The first is the spectra and spatial distribution per maser species toward the HII regions; the second involves the CH_3OH maser emission toward a region with weak background continuum radiation. In addition, we present a tool for modeling and fitting the unsaturated molecular maser signals with non-LTE radiative transfer models and Bayesian analysis using the Markov-Chain Monte Carlo (MCMC) approach.

2. Maser Emission associated with H II Regions

2.1. *CH_3OH $5_{-1}-4_0$ Transition at 84 GHz*

We present the first detection of the 84 GHz Class I CH_3OH masers toward Sgr B2 with interferometric ALMA observations at a resolution of 1.5″. The brightest maser spot located ∼3.6″ west of the K4 cm-wave core with a $V_{\rm lsr}$ of 58 km s^{-1} has a peak brightness temperature ($T_{\rm B,\,peak}$) of 389.2 ± 0.2 K. In addition to the brightest spot, another maser knot associated with the K6 HII region is also identified with a $T_{\rm B}$ of 75.4 ± 0.4 K at a $V_{\rm lsr}$ of 83 km s^{-1} (hereafter referred to as CH_3OH-83 km s^{-1} spot).

The spectra extracted toward the CH_3OH-83 km s^{-1} maser spot are shown in Fig. 1 (top) with two distinct velocity components being identified. A chained two-component model is constructed to iteratively generate synthetic spectra, each component being described with five parameters, $T_{\rm k}$, $n_{\rm c}$, $V_{\rm lsr}$, dV and $N_{\rm col}$. This maser spot is aligned with the K6 HII region, which provides background radiation to be amplified by the stimulated emission. Taking into account $T_{\rm cont}$, there are 11 free parameters in total to be adjusted in the MCMC analysis. All parameters converge to primarily Gaussian distributions in our model. The nominal mean for each parameter from the MCMC inference is used to construct the synthetic spectra shown in Fig. 1 (top), which

https://doi.org/10.1017/S1743921323002636 Published online by Cambridge University Press

fit satisfactorily with the observed spectra when noise levels are taken into account. The excitation temperature and opacity of the $5_{-1} - 4_0$ maser transition are found to be negative, with a $T_{\rm ex}$ and τ being -5.6 K and -2.5 for the high velocity component.

2.2. *CH_2NH $1_{1,0} - 1_{1,1}$ Transition at 5.29 GHz*

The maser activity of the CH_2NH transitions at 5.29 GHz has been revealed toward both the Galactic Center and external galaxies as point source emission (Faure et al. 2018; Gorski et al. 2021). With the VLA observations, we resolve this maser emission spatially into three velocity components with a $V_{\rm lsr}$ of 64, 73, and 83 km s^{-1}. The 83 km s^{-1} and 64 km s^{-1} components are both associated with the K6 HII region, with the brightest 83-km s^{-1} component displaying a compact distribution with a $T_{\rm B,\,peak}$ of 121.8 ± 8.6 K. The VLA observations are insufficient to simultaneously constrain all the physical characteristics so the CH_2NH MCMC analysis requires a confined choice of priors on some parameters. We opted to use CH_3OH discussed in Sec. 2.1 for physical constraints as the 83 km s^{-1} components of CH_3OH and CH_2NH are spatially coherent and are both associated with K6 HII region. We therefore extracted the CH_2NH spectrum toward the same position of the CH_3OH-83 km s^{-1} maser spot. The posteriors on $T_{\rm k}$ and $n_{\rm H_2}$obtained from CH_3OH are adopted as the priors for the CH_2NH model. The samplers converge at a $N_{\rm col}$ of $\sim 5 \times 10^{14}$ cm^{-2}. The six hyperfine components of the $1_{1,0} - 1_{1,1}$ transition have $T_{\rm ex}$'s in the range of -0.75 – -0.55 K, τ's in the range of -0.03 – -0.006.

2.3. *CH_2NH_2 $2_0 - 1_1$ E Transition at 4.36 GHz*

The CH_2NH_2 transition at 4.36 GHz displays maser activity similar to the 5.29 GHz CH_2NH transition. Three velocity components were resolved for the CH_2NH_2 maser emission, with a high degree of morphological consistency with the CH_2NH maser. However, a lack of molecular collisional data for CH_2NH_2 prevents us from interpreting the spectral profiles. Future quantum mechanical calculations of the cross sections and rate coefficients of CH_2NH_2 will provide vital information for constraining its excitation conditions and pumping mechanism.

2.4. *Spatial Origin and Pumping Mechanism*

By scrutinizing the VLA and ALMA observations, we found that the K6 HII region harbors maser emission of Class I CH_3OH at 84 GHz, CH_2NH at 5.29 GHz, and CH_2NH_2 at 4.36 GHz (Fig. 2). The 83-km s^{-1} spot of the CH_2NH and CH_2NH_2 masers at K6 remarkably resembles those of the Class I CH_3OH maser. Their consistent morphology serves as strong evidence to support a similar collisional pumping mechanism for the CH_2NH and CH_2NH_2 masers with the Class I CH_3OH maser as well as a common physical condition for triggering these masers. In addition, these maser activities toward the K6 region might also imply the occurrence of energetic events in the masing regions, considering that K6 was recognized as the ionization front of the HII regions and located far from strong infrared sources (Gaume et al. 1995). By understanding the conditions that are necessary for maser activities to occur, we can also better understand how they can be used to monitor astronomical objects. For example, since these new masers are pumped by intense collisions, we can expect them to be good candidates for monitoring regions with time-dependent gas dynamics, such as episodic outflows from massive protostars and accretion disks in extra-galactic environments.

https://doi.org/10.1017/S1743921323002636 Published online by Cambridge University Press

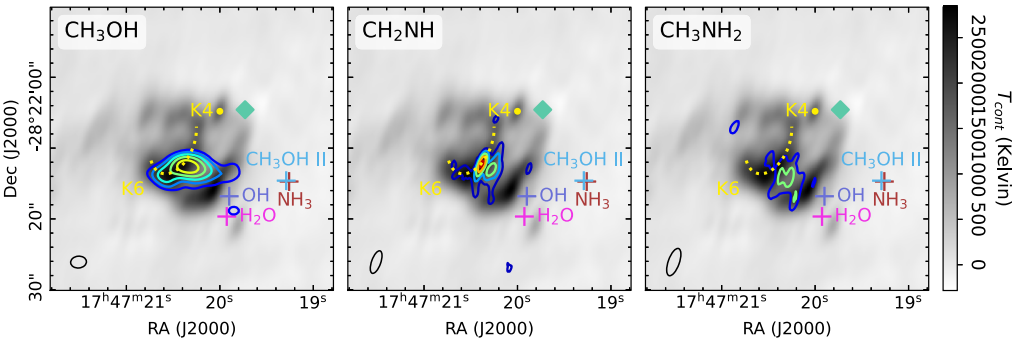

Figure 2. The 83-km s^{-1} components of the 84 GHz Class I CH_3OH maser, 5.29 GHz CH_2NH maser, and 4.36 GHz CH_2NH_2 maser are shown with contours and superimposed on the free-free continuum emission at 6.8 cm. The brightest 84 GHz Class I CH_3OH maser spot is marked with a diamond symbol while the brightest maser spots of OH, H_2O, NH_3, and Class II CH_3OH masers are marked with + symbols (Argon et al. 2000; Caswell et al. 2010; Walsh et al. 2014; Yan et al. 2022). The arc-like K6 H II region is marked with a yellow dotted line.

3. Maser Emission against Weak Background Radiation

In contrast to the CH_3OH-83 km s^{-1} maser spot, there is no significant mm-wave continuum source at the brightest CH_3OH maser spot (shown with a diamond symbol in Fig. 2). While this spot also exhibits a strong CH_3OH emission at 44 GHz (Mehringer & Menten 1997), it shows no continuum emission at cm-wave either. The closest continuum source, K4, is offset by $\sim 3.6''$ which corresponds to $\sim$0.14 pc at the distance of Sgr B2 (8.2 kpc, Reid et al. 2019). In addition, the nearest bright infrared source observed with both the 2MASS and the GLIMPSE program is located at $\sim 5.2''$ to the west of the maser spot.

The model we consider here consists of double masers, where two masing clumps along the line of sight overlap in velocity. The weak continuum radiation is first amplified by the background masing clump, which is then further amplified by the foreground masing clump. This double-masing-clump model could account for the strong maser emission with an absence of a bright continuum source. It is analogous to the "self-amplification" model of two masing clouds that has been used to interpret water megamasers observed in circumnuclear disks in active galactic nuclei (Kartje et al. 1999). We processed the spectral analysis assuming that the only source of continuum is the cosmic microwave background. Each of the spectral features consists of two individual velocity components, which have coherent but not identical $V_{\rm lsr}$ of $\sim$58 km s^{-1} although spatially separated. As shown in Fig. 1 (bottom), the constructed profiles fit reasonably well with the observed spectra for both the maser and the optically thick emission features. The $T_{\rm ex}$ and τ of the $5_{-1} - 4_0$ maser transition are found to be -271.4 K and -0.3 for the background clump and -7.9 K and -1.4 for the foreground clump.

4. Conclusion

We report interferometric observations of maser activity from large molecules toward Sgr B2 using ALMA and VLA. Enabled by the ALMA observation, we report the first detection of the Class I CH_3OH maser at 84 GHz toward Sgr B2. Multiple 84 GHz CH_3OH maser knots are resolved with a $T_{\rm B,\,peak}$ of 389.2 ± 0.2 K at a velocity of 58 km s^{-1}. With the VLA observations, we characterize the spatial origin of the 5.29 GHz CH_2NH maser and the 4.36 GHz CH_2NH_2 maser. We found a definite association between the maser emission from these large molecules and the UC HII region. They are offset from the masing regions of the radiatively pumped maser species and the infrared sources. In

https://doi.org/10.1017/S1743921323002636 Published online by Cambridge University Press

contrast, the spatial correlation between the activities of the new masers suggests that the CH_2NH and CH_2NH_2 masers are pumped by intense collisions, analogous to the Class I CH_3OH maser. By understanding the nature of the new maser species, we can better understand how they may serve as good candidates for monitoring astronomical objects with time-dependent gas dynamics.

References

Argon, A. L., Reid, M. J., & Menten, K. M. 2000, *ApJS*, 129, 159
Caswell, J. L., Fuller, G. A., Green, J. A., *et al.* 2010, *MNRAS*, 404, 1029
Cyganowski, C. J., Brogan, C. L., Hunter, T. R., *et al.* 2009, *ApJ*, 702, 1615
Chen, X., Sobolev, A. M., Ren, Z.-Y., *et al.* 2020, *Nature Astronomy*, 4, 1170
Faure, A., Remijan, A. J., Szalewicz, K., *et al.* 2014, *ApJ*, 783, 72
Faure, A., Lique, F., & Remijan, A. J. 2018, *The Journal of Physical Chemistry Letters*, 9, 3199
Kartje, J. F., Königl, A., & Elitzur, M. 1999, *ApJ*, 513, 180
Gaume, R. A., Claussen, M. J., de Pree, C. G., *et al.* 1995, *ApJ*, 449, 663
Gorski, M. D., Aalto, S., Mangum, J., *et al.* 2021, *A&A*, 654, A110
Mehringer, D. M. & Menten, K. M. 1997, *ApJ*, 474, 346
McGuire, B. A., Loomis, R. A., Charness, C. M., *et al.* 2012, *ApJL*, 758, L33
Reid, M. J., Menten, K. M., Brunthaler, A., *et al.* 2019, *ApJ*, 885, 131
Walsh, A. J., Purcell, C. R., Longmore, S. N., *et al.* 2014, *MNRAS*, 442, 2240
Yan, Y. T., Henkel, C., Menten, K. M., *et al.* 2022, *A&A*, 666, L15